Biomed Microdevices (2010) 12:1001–1008
DOI 10.1007/s10544-010-9454-x

A microfluidic traps system supporting prolonged culture of human embryonic stem cells aggregates

Maria Khoury · Avishay Bransky · Natanel Korin · Limor Chen Konak · Grigori Enikolopov · Itai Tzchori · Shulamit Levenberg

Published online: 28 July 2010

Abstract The unlimited proliferative and differentiative capacities of embryonic stem cells (ESCs) are tightly regulated by their microenvironment. Local concentrations of soluble factors, cell-cell interactions and extracellular matrix signaling are just a few variables that influence ESC fate. A common method employed to induce ESC differentiation involves the formation of cell aggregates called embryoid bodies (EBs), which recapitulate early stages of embryonic development. EBs are normally formed in suspension cultures, producing heterogeneously shaped and sized aggregates. The present study demonstrates the usage of a microfluidic traps system which supports prolonged EB culturing. The traps are uniquely designed to facilitate cell capture and aggregation while offering efficient gas/nutrients exchange. A finite element simulation is presented with emphasis on several aspects critical to appropriate design of such bioreactors for ESC culture. Finally, human ESC, mouse Nestin-GFP ESC and OCT4-EGFP ESCs were cultured using this technique and demonstrated extended viability for more than 5 days. In addition, EBs developed and maintained a polarized differentiation pattern, possibly as a result of the nutrient gradients imposed by the traps bioreactor. The novel microbioreactor presented here can enhance future embryogenesis research by offering tight control of culturing conditions.

Keywords Microfluidics · Micro-Bio reactor · Embryonic stem cells · Embryoid bodies

Maria Khoury and Avishay Bransky equally contributed.

M. Khoury · A. Bransky · N. Korin · L. C. Konak · I. Tzchori · S. Levenberg (✉)
Biomedical Engineering,
Technion,
Haifa, Israel 32000
e-mail: shulamit@bm.technion.ac.il

G. Enikolopov
Cold Spring Harbor Laboratory,
Cold Spring Harbor, NY 11724, USA
e-mail: enikolop@cshl.edu

1 Introduction

Embryonic stem cells (ESCs) bear great therapeutic potential in tissue engineering techniques and regenerative medicine due to their unlimited proliferative capacity and ability to differentiate into each of the three embryonic germ layers (Solter and Gearhart 1999; Thomson et al. 1998). ESCs can form any cell type, unlike stem cells isolated from adult tissue, which are more limited in their repertoire of potential cell types (Odorico et al. 2001). A method commonly used to initiate ESC differentiation is based upon cell aggregation and formation of three dimensional colonies known as embryoid bodies (EBs) (Keller 1995; Itskovitz et al. 2000). This method of differentiation closely mimics embryonic processes, where early development and germ layer formation are partially recapitulated. Within the first few days of differentiation, EBs generate cell populations of primitive endoderm, ectoderm and mesoderm lineages, while over more extended culture periods, hematopoietic, endothelial, muscle and neuronal cells can already be detected (Keller 1995).

Cell lineage profiles can vary dramatically between EBs grown within the same culture. Most likely, slight differences in the microenvironment of individual EBs govern differentiation of cell subsets within the structure, which can then further guide the differentiation of neighboring cells. Such influences can be mediated via cell-cell contact or secretion of soluble factors (Watt and

Hogan 2000), as has been described for ESC differentiation in vivo (Spradling et al. 2001).

EB size has been reported to directly affect differentiation, as a minimum number of cells were required to form EBs designed to induce differentiation of hematopoietic cells (Ng et al. 2005). Similarly, EB shape plays a critical role in differentiation fate, as shown by extended pluripotency and self renewal of EBs grown in microwells when compared to unconstrained EBs (Mohr et al. 2006). Control of EB size can be directed toward the initial aggregation period (Ungrin et al. 2008; Karp et al. 2007; Park et al. 2007) or toward prolonged culture periods (Mohr et al. 2006; Moeller et al. 2008), in direct correlation with microwell incubation lengths (Hwang et al. 2009).

In addition, the oxygen tension microenvironment can significantly influence EB differentiation. Hypoxic conditions are common to developing embryos, where cells respond by stimulating several hypoxia-inducible factors (HIF) (Simon and Keith 2008). Genetic studies of these factors have shown their key role in regulation of ontogeny. Oxygen concentrations have been shown to affect cardiovascular morphogenesis (Shweiki et al. 1992), mammalian placentation (Adelman et al. 2000), bone morphogenesisn (Rajpurohit et al. 1996) stem cell fate (Morrison et al. 2000). Therefore manipulation of the geometric and atmospheric microenvironment of EBs can directly control their differentiation fate and may correlate with in vivo embryonic differentiation.

Microfabrication technology enables such fine-tuned culture management by means of control and reproducibility of extracellular cues to levels unachievable by standard tissue culture (El-Ali et al. 2006; Villa-Diaz et al. 2009). Microfabricated cell cultures, also referred to as micro-bioreactors, have been utilized to study cell function under shear (Korin et al. 2007), differentiation of C2C12 cells (Tourovskaia et al. 2005) and hepatocyte morphogenesis (Powers et al. 2002). However, in such culture setups, non adherent cells, such as the EBs, should be trapped within the micro-bioreactor to prevent them from being washed out and thus setting the environment to one given location. Wu et al. (Wu et al. 2008) have demonstrated a microfluidic platform for culturing of tumor spheroids. Their device enabled the aggregation of single cells inside microtraps and their culture under perfusion conditions for 24 h. Similar experimental setups have been demonstrated for adherent HeLa cells (Di Carlo et al. 2006) and for ESC fusion studies (Skelley et al. 2007). However these techniques fail to regulate oxygen levels as required for EB culturing designed for embryogenesis-mimicking research protocols.

The present study demonstrates application of a novel micro-bioreactor tailored to enable prolonged EB culturing. The bioreactor includes thousands of microtraps facilitating single ESC positioning for aggregation initiation and prolonged culturing. When compared to micro-wells or early trap-like constructions where most of the ESCs have no contact with the medium, the unique microtrap design provides optimized conditions for the sensitive EBs, allowing initial coalescence of multiple cells and improved gas exchange and accessibility to nutrients. In contrast to micro-well culturing conditions, EB size is constrained in all orientations, as the constant medium flow inhibits EB growth beyond the trap opening. In addition, a uniform number of cells initiates aggregate formation due to the trap geometry which ensures its complete filling.

Finite element simulations of the fluid flow, oxygen convection and consumption by the EBs are presented. The simulations results provide insight into the mechanisms involved in loading of the cells and the following gas exchange. A comparison is made between the specially designed trap and a simple design whereby the first proves crucial for cell viability. In addition, this setup demonstrates enhanced EB differentiation with exposure to oxygen and nutrient gradients spatially correlating with low oxygen concentrations. More specifically, differentiation cues were most pronounced at the inner portions of the microtrap, when compared to those stimulating cells along the trap perimeter and exposed to constant medium flow. In this manner, the novel micro-bioreactor detailed here enables monitoring of cell differentiation in relation to oxygen and soluble factor gradients and may serve for further investigation of the role of microenvironments on ESC differentiation and for propagating uniform EB cultures.

2 Experimental

2.1 Device fabrication

The microfluidic device was fabricated in PDMS using soft lithography techniques as described before (Bransky et al. 2008). Briefly, silicon masters were fabricated using lithography of SU-8 photoresist (2075, Microchem Corp., Newton, MA). The SU-8 was spun on to the silicon wafer producing a layer of 50 μm in thickness and then baked, exposed, rebaked and developed. The master was dried and silanized overnight in vacuum using trimethylchlorosilane (Sigma Aldrich). As the features of the mask are intricate and require high aspect ratio, the protocol required many optimizations until reaching the desired result.

The silicon master was placed at the bottom of a Teflon mold and tubes were inserted through the mold defining the inlets and outlets to the device. A PDMS mixture (Sylgard 184, Dow Corning, Midland, MI) was poured into the mold which was kept at 70°C for 2 h. After curing, the PDMS slab was peeled off the mold and the tubes were extracted. The PDMS slab was then sealed using oxygen plasma to glass slide 76×50×1 mm (Marienfeld, Germany) spun

coated with PDMS. In this way, the EBs could not adhere to any surface of the microfluidic device during the culturing period.

The fluidic network comprised eight main interconnected microchannels connected such that each has the same flow resistance (Fig. 1). Through division of the area into separate flow regions, a more homogeneous spreading of cells upon seeding can be attained, together with heightened flow uniformity. Additionally, the walls between the microchannels provide mechanical support preventing PDMS bloating. The entry point to each microchannel was equipped with a cylindrical cavity designed to capture small bubbles that escaped the main bubble trap.

2.2 Cell culture

Human ESCs (hESC, H9 clone) and H1 Oct4-EGFP (WiCell) were grown on mouse embryonic fibroblasts (MEF) in culture medium prepared from 80% DMEM/F-12 (Biological Industries) and 20% KnockOut SR (Gibco), supplemented with 1 mM nonessential amino acids (Gibco), 1 mM glutamine (Gibco), 0.1 mM β-mercaptoethanol (Gibco) and 4 ng/ml basic fibroblast growth factor (bFGF; PeproTech). Tissue culture plates were coated with 0.1% gelatin (Sigma) before being seeded with hESC, then cultured in 5% CO_2 and routinely passaged every 5–6 days.

EB formation within the microfluidic device was induced by digestion of hESC colonies with 1 mg/ml collagenase type IV (Gibco) before passing the cells through a 70 μm filter (BD Falcon). The cells were then injected into the traps, positioned on the microscope stage, using a syringe.

The device was then connected to the perfusion system which included a syringe pump (KDS210, KDS Scientific), bubble trap (Scientific Systems, Inc.), gas permeable tube (1-m long, 1 mm ID, 1.3 mm OD, Silastic ® tube, Cole-Parmer) and a waste container. The apparatus (apart from the syringe pump) was kept in an incubator for 5–7 days, infusing at flow rates ranging from 0.2 to 0.5 ml/h.

2.3 Mouse GFP-ESC and EB formation

Mouse Nestin-GFP ESCs (Gleiberman et al. 2005) were grown on mitomycin-C-treated, neomycin-resistant primary embryonic fibroblasts (MEFs; Chemicon, Millipore Corporate, MA), seeded on 100-mm tissue culture dishes (Millipore) in Dulbecco's Modified Eagle's Medium (DMEM) (Gibco, Carlsbad, CA) supplemented with 15% fetal bovine serum (HyClone Laboratories, Logan), 2 mM L-glutamine, 1 mM sodium pyruvate, 0.1 mM β-mercaptoethanol, 0.1 mM nonessential amino acids, 50 U/ml penicillin/50 μg/ml streptomycin (Gibco), and 1,000 U/ml leukemia inhibitory factor (LIF, Chemicon, Temecula, CA). mESC colonies were digested and injected to the microfluidic device to form EBs, as described for hESCs.

2.4 Numerical simulations

Oxygen and nutrient levels present limiting factors in microdevices of this nature, due to the high surface area to volume ratios. Thus, it is important to construct an appropriate mass transport model to ensure cell survival and normal growth. The model for oxygen is based on the mass continuity equation for a dilute solution and the steady state Navier-Stokes equation for a Newtonian fluid.

The following convective diffusion equations were solved for the specific microdevice geometry, using a finite element simulation (COMSOL Multiphysics 3.3):

$$\rho_f\left(\frac{\partial \vec{u}}{\partial t}+\vec{u}\cdot\nabla\vec{u}\right)=-\nabla P+\mu\nabla^2\vec{u} \tag{2.1}$$

$$\nabla\cdot(-D\nabla c)=R-\vec{u}\cdot\nabla c \tag{2.2}$$

where D is the isotropic diffusion coefficient of oxygen in water, c—concentration, u—velocity field, R—oxygen consumption rate of the cells, P—pressure, ρf—fluid density and μ—fluid viscosity.

The values used in the simulation are summarized in Table 1.

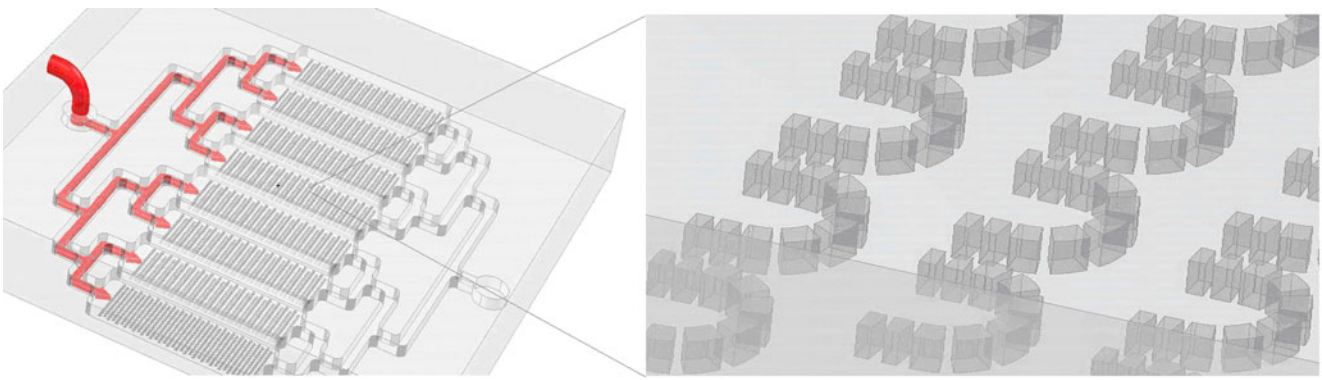

Fig. 1 The micro-bioreactor setup: an illustration of the microfluidic device on the left and a zoom in on the microtraps on the right

Due to the symmetry of the problem half of a single micro-trap containing a spheroid aggregate was modeled inside a microchannel. No slip boundary condition was chosen for the channel walls and EB surface. A constant velocity in the flow direction was imposed at the inlet with zero pressure at the outlet. Zero mass flux was imposed on all surfaces except for the EB.

The oxygen consumption rate (OCR) for the EB bulk was set according to Michaelis-Mentin kinetics with respect to oxygen concentration (Cochran et al. 2006; Korin et al. 2009):

$$OCR = V_{\max}\frac{C}{C + K_m} \tag{2.3}$$

Where C denotes the oxygen concentration, Vmax—the maximum consumption rate and Km - Michaelis-Mentin constant. At high oxygen concentrations (C>>Km), the OCR approaches a constant value Vmax, whereas at low concentrations, the OCR approaches zero.

The medium at the inlet was assumed to have constant oxygen concentration.

In order to simulate the loading of cells onto the trap, Eq. 2.1 was solved separately for the case where no aggregate is present for both a segmented trap and a solid one.

3 Results and discussion

3.1 Numerical simulation

The traps design described above is advantageous for both the cell loading and culturing stages. The gaps between the segments of the trap are in the order of the cells size (7 μn) thus single cells or small aggregates arriving at the trap tend to block these gaps. As the trap fills with cells, gaps at the base of the trap remain open, allowing streams to pass through the trap. These streamlines continue to deliver cells until the trap is completely full.

Figure 2 left illustrates the stream lines which develop when loading of a standard nonsegmented trap. Due to the negligible inertia effects, the cells precisely follow streamlines and are therefore never trapped. However, when simulating cell loading for the segmented trap, streamlines pass through the trap enabling cell entrapment (Fig. 2 right).

Oxygen is the most vital of nutrients and an important modulator of cellular function. Hypoxic responses (5–15 $mmHgO_2$) lead to anaerobic metabolic processes and usually, for normal culture protocols, oxygen should be sustained above this level (Roy et al. 2001).

Specifically for ESC the oxygen level and its variance across the aggregate should be well defined, as they affect cell proliferation and differentiation mechanisms.

Oxygen transport simulation performed for both a segmented and standard trap are shown in Fig. 3(a and b), respectively. The segmented trap significantly enhances gas exchange with the surrounding medium, via streamlines which traverse the trap, delivering nutrients and oxygen and disposing of CO_2. Figure 3 illustrates three typical oxygen concentration slices of the two trap geometries infused at a flow of 0.2 ml/h (0.4 mm/s). As no streamlines pass through the solid trap, cells exhaust oxygen near the inner part of the trap. In contrast, the segmented trap allows for medium flows around the EB, providing for effective mass transport.

Oxygen concentration along the center line crossing the EB is plotted in Fig. 4 for the two trap geometries at different flow rates. Oxygen level in the unsegmented trap dip to a minimum of 3.5 e–3 mol/m3 (2 mmHg), whereas concentrations at the segmented trap remain above 0.11 mol/m3 (64 mmHg). Thus, portions of EBs cultured in standard traps will be subjected to hypoxic condtions and will most likely become necrotic. As the flow rate increases the oxygen concentration increases due to a stronger convective flux in the segmented geometry as opposed to the solid geometry where the change is negligible.

Table 1 Simulation parameters

Parameter	Description	value
D_{O2T}	Oxygen diffusion coefficient in EB (tissue) at 37°C	2×10^{-5} cm^2/s [33]
D_{O2W}	Oxygen diffusion coefficient in water 37°C	2×10^{-5} cm^2/s
C_{in}	Inlet oxygen concentration	0.19 mol/m^3
v_{mean}	Mean fluid velocity	0.1 mm/sec
ρ	Water density	1 kg/m^3
μ	Viscosity of water	1 mPas
h	Channel height	50 μm
w	Channel width	3 mm
D	Trap width	200 μm
V_{max}	Maximum oxygen consumption rate	4×10^{-17} mol/cell/s [31]
K_m	Michaelis-Mentin constant	5.2 mmHg [31]

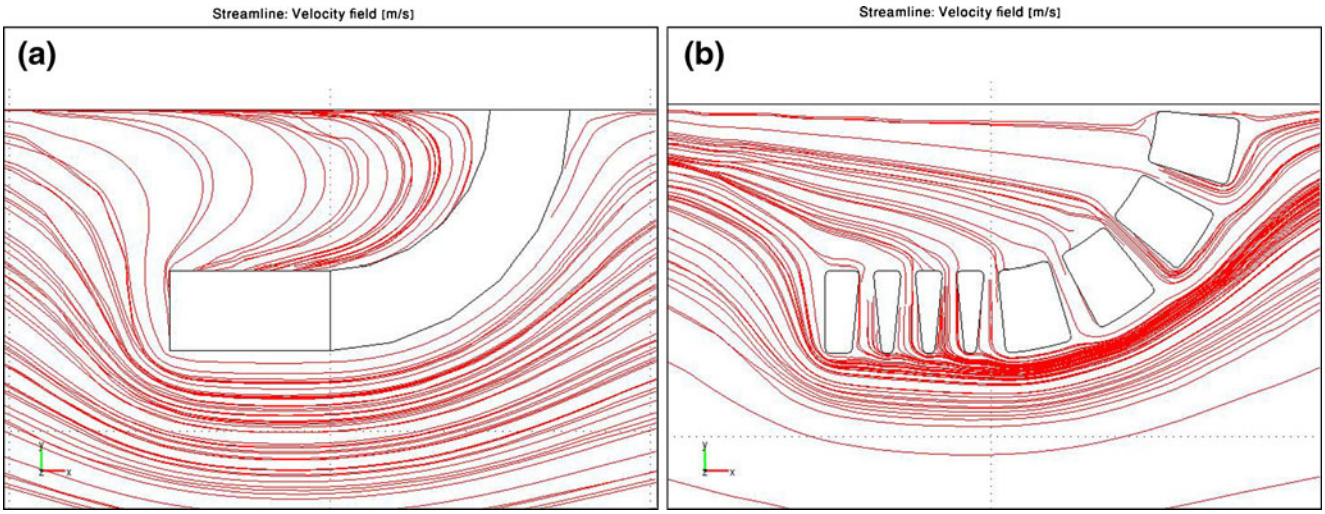

Fig. 2 Nonsegmented and segmented trap stream lines. The streamlines solution for the regular trap design (**a**) and the segmented trap design (**b**). The streamlines which cross the trap through the gaps enable the trapping of the cells which otherwise leave the trap as in A

3.2 Human EB (hEB) culture in microtraps

In order to study the behavior of human EBs in the microfluidic devices, fragments of hESC colonies were seeded in the microtraps and cultured for 6 days. The aggregates attained the familiar shape of an EB within 2–3 days and did not grow significantly during this period.

Two trap sizes were used: 100 μm and 200 μm diameter in order to evaluate the size constraint effect on the EB (Fig. 5(a,b)). Aggregates were formed in both trap sizes and maintained their size without growing out of the trap region. As no significant differences were noted between the two trap geometries, all later experiments were performed in 200 μm microtraps, a size closely resembling that of 5–6 day old EBs. hEB viability was determined after 3 days in culture and confirmed that the vast majority of the EB was made of live cells (Fig. 5(c)). A number of dead cells and debris were detected on the EBs or trap, introduced by the system's continuous flow.

ESC differentiation often involves the formation of cell aggregates (EBs). These EBs are typically made from suspension cultures resulting in heterogeneous structures

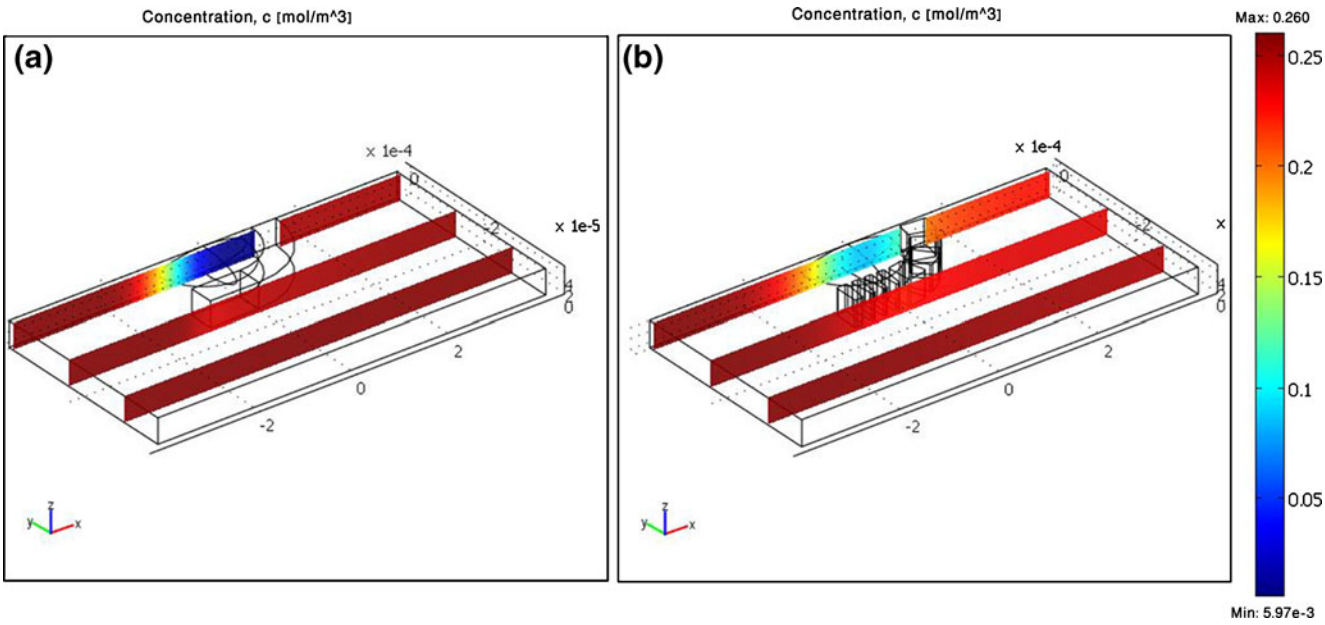

Fig. 3 Gas exchange modeling of segmented and nonsegmented microtraps. The results obtained for the convection diffusion problem of the standard trap (**a**) and the segmented trap (**b**). The more efficient gas exchange present in the latter is found vital for cell survival as oxygen concentration remain above the hypoxia level

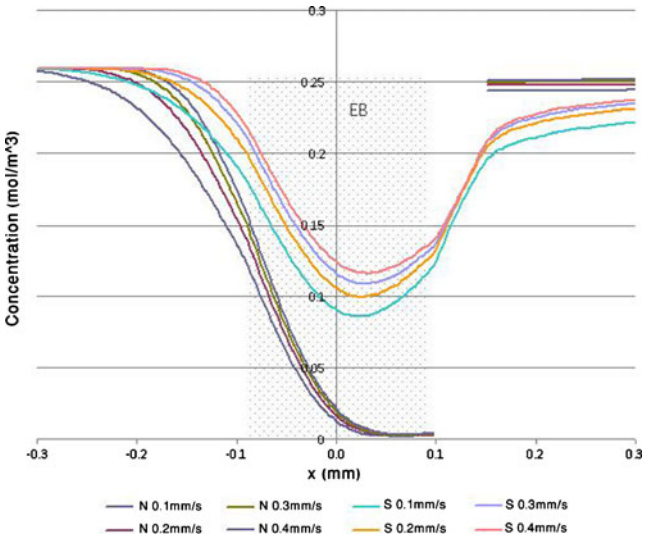

Fig. 4 Oxygen concentrations measured across EBs in segmented and nonsegmented traps. The oxygen concentrations along the center line crossing the EB (textured rectangle) for four mean velocities: 0.1, 0.2, 0.3 and 0.4 mm/sec as obtained for the segmented trap (S) and normal trap (N). The concentration of oxygen near the trap openings increases slightly with increasing flow rate. Increasing the flow rate will not prevent the cells from reaching hypoxia in the solid trap

with a wide range of sizes and shapes. In order to recapitulate the developmental processes of early hESC differentiation, it is crucial to possess the tools to generate spatially and temporally synchronized hEBs. Recently, a number of methods have been developed to allow for control of EB size and shape. Ungrin et al. (Ungrin et al. 2008) demonstrated that a centrifugal forced-aggregation strategy can lead to formation of well-defined aggregates promoting survival of hESCs with ROCK inhibitor. Another study used microfabricated adhesive stencils to define the initial geometry of the ESC colony. Functional studies performed on EBs formed in this manner, report that similar differentiation rates were recorded for both EBs and 300 μm aggregates, suggesting that natural differentiation mechanisms can be incurred in micropatterned 300 μm aggregates (Park et al. 2007). An additional approach utilized microwell arrays fabricated in poly(ethylene glycol) (PEG) which reduced non-specific cell adhesion enabling culture of homogeneously sized EB populations. The authors claim the method is superior to suspension culture methods in controlling the homogeneity of EB populations (Moeller et al. 2008). Although the referenced methods can control the initial size and shape of EBs, they fail to maintain EB microwell culture for prolonged periods. In contrast, microfluidic traps support cell viability over time and enhance cell differentiation within the traps for more than 5 days. Furthermore, nutrient gradients across the microtrap region can be controlled by varying flow rates and initial oxygen concentrations, as demonstrated in the simulation described earlier. The latter cannot be achieved via static culture conditions, as diffusion serves as the sole mass transport mechanism.

3.3 Differentiation of mESC cultures in segmented microtraps

A mESC line expressing the enhanced green fluorescent protein (EGFP) under the control of the fluorescently-tagged nestin promoter (Nestin-GFP) was used to evaluate the influence of trap geometry and flow conditions on ESC differentiation. mEBs cultured using the hanging drop (HD) method, failed to express detectable levels of Nestin-GFP within the first 3 days in culture (Fig. 6(a)). However, from days 4 and 5, GFP expression was detected in EBs formed using the HD method as well as standard aggregates methods (data not shown). mEBs treated with retinoic acid (RA) show robust GFP expression, indicating elevated expression of Nestin starting from day 2 (see Fig. 6(b)). In the presence of RA, a high percentage of cells within the EB retained elevated GFP levels for more than 6 days.

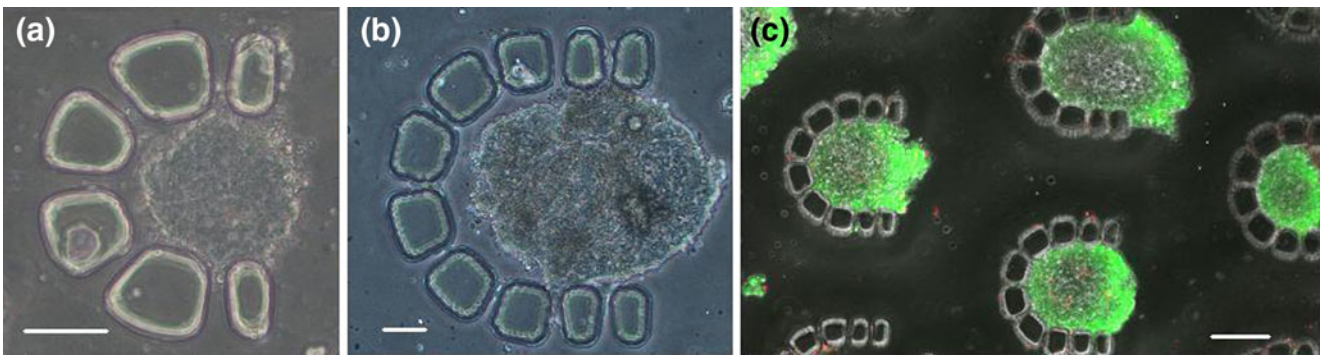

Fig. 5 hEBs culture in segmented microtraps. Bright field images of hEBs formed and cultured in 100 μm (**a**) and 200 μm (**b**) diameter microtraps. (**c**) Viability assay of hEBs cultured in 200 μm diameter microtraps for 3 days. Live cells are stained green and dead cells are stained red. Note that staining efficiency decreased towards the back of the trap due to its diffusion limited nature, however no dead cells are present, as the oxygen levels were sufficient. Scale bars: 50 μm (**a**, **b**) and 100 μm (**c**)

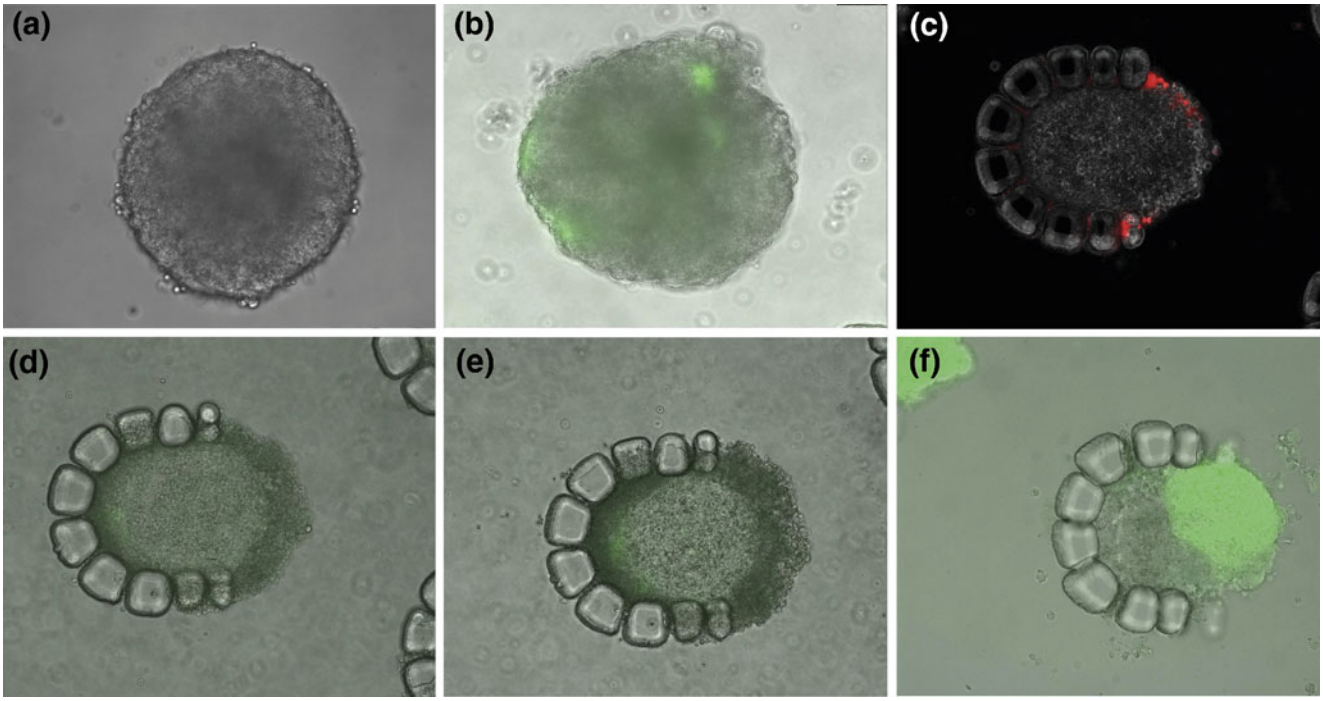

Fig. 6 mESC-EB culturing and differentiation in segmented microtraps. mEB cultured for 3 days according to the HD method in the absence (**a**) or presence (**b**) of RA. (**c**) Cell viability assay performed on an mEB. (d) Sequential pictures of a Nestin-GFP-mEB cultured in a microtrap at day 3 (**d**), and day 4 (**e**). (**f**) Oct4-GFP-hEB cultured in a microtrap for 2 days

mEBs cultured in microtraps were then monitored for Nestin expression with emphasis on recording of differential expression patterns within the trap. Fragments of mESC colonies were seeded in the microtraps and cultured for up to 6 days. The microaggregates assumed the familiar EB shape within 1–2 days and remained viable within the microtraps (Fig. 6(c)). mEB positioning within the microtraps proved influential on cell differentiation fate, as GFP expression was detected from day 3 in culture, but only by cells situated at the inner rim of the microfluidic traps (Fig. 6(d)). Cells neighboring the trap opening failed to express Nestin-GFP and retained OCT4-GFP expression (Fig. 6(e)), suggesting a slower rate of differentiation. Patterned GFP expression was not detected in EBs prepared via the HD, aggregates or HD+RA methods.

These results stand in line with previous works which showed expression of ectoderm, mesoderm and endoderm markers upon removal of LIF from mESC-EB microwell cultures (Karp et al. 2007), while maintained LIF concentrations supported expression of undifferentiated markers, such as SSEA-1. Similar results were reported for hESCs cultured in MEF-conditioned medium supplemented with bFGF which maintained viable and undifferentiated cells for weeks of culture (Mohr et al. 2006).

The present work demonstrates that ESC aggregates can asymmetrically differentiate in relation to their location within the microfluidic trap, and in close correlation with the state of the culture medium. In contrary to previous works that demonstrated uniform EB differentiation according to the culture medium, as shown by Karp et al. (Karp et al. 2007) and Mohr et al. (Mohr et al. 2006), the microfluidic culturing method, creates nutrient concentration gradients that affect the typical radial symmetry (Fig. 4) and can thereby inhibit differentiation on one side of the EB while stimulating it on the other.

Cells located at the inner parts of traps, as opposed to their counterparts at the trap openings, are exposed to lower nutrient levels and are most likely to be exposed to higher concentrations of excreted factors. These conditions are most likely responsible for the noted differences in Nestin-GFP and OCT4-GFP expression across the trapped EB.

Furthermore, serum starvation has been shown to reduce ESC proliferation rates (Gassmann et al. 1996), which can further explain the differential ESC behavior throughout the microtrap. ESCs located at the inner parts of the trap are exposed to lower concentrations of serum which can hinder cell cycle progression, rendering them more sensitive to internally secreted differentiation cues. Medium flow can also promote asymmetric differentiation within the microtrap, as shear stress has been recognized as a critical regulator of cellular differentiation in mesenchymal stem cells (Provot et al. 2007).

EB growth patterns have been shown to be identical under both 20% (normoxia) and 1% (hypoxia) conditions during the first 5 days of differentiation (Gassmann et al. 1996). However, more recent works have demonstrated that

multiple stem or progenitor cell populations are influenced by oxygenation levels, via O_2-sensitive intracellular pathways which regulate cell fate (Johnson 2009). Furthermore, while Ezashi et al. (Ezashi et al. 2005) reported similar proliferation rates for hESCs cultured under hypoxic and normoxic conditions, of the number of differentiated regions was substantially reduced under hypoxic conditions. Thus, the authors concluded that hypoxic conditions are required to maintain the full pluripotency of mammalian ESCs.

The results shown here do not necessarily contradict previous findings where differentiation was inhibited by low oxygen concentrations as the oxygen concentration decreases only by a maximum of 50% in the trap (Fig. 4). The polarized state of the EBs may be caused by the oxygen gradient, by increased concentration of cell excreted factors inside the trap or by the lack of nutrients as was discussed above.

In this manner, microtraps can mimic polarization innate to embryogenesis (see review by Johnson 2009). Most of the cells at the eight-cell stage of an early embryo become polarized and develop tight junctions with the other cells, leading to development of polar cells on the outer rim and apolar cells at the aggregate core. Thus, the microtrap culturing method can be offer tools to foster our understanding of early embryogenic process by allowing for cell-polarization.

4 Conclusions

In summary, hESC culturing in microfluidic traps offers the advantages of tight control of nutrient flow and medium composition, facilitating directed and temporal stimuli over the microtrap. Flow rates and initial nutrient concentrations can be manipulated, enabling fine-tuning of EB growth conditions and stimulating differential behavioral responses. In addition, as each aggregate is located at a defined position, automated microscope stages and image processing can be used to monitor each one over time. Thus, this platform may be beneficial in furthering future ESC research.

References

D.M. Adelman, M. Gertsenstein, A. Nagy, M.C. Simon, E. Maltepe, Genes Dev. **4**(24), 3191–3203 (2000)

A. Bransky, N. Korin, S. Levenberg, Biomed. Microdevices **10**(3), 421 (2008)

D.M. Cochran, D. Fukumura, M. Ancukiewicz, P. Carmeliet, R.K. Jain, Ann. Biomed. Eng. **34**(8), 1247–58 (2006)

D. Di Carlo, L.Y. Wu, L.P. Lee, Lab Chip **6**(11), 1445–49 (2006)

J. El-Ali, P.K. Sorger, K.F. Jensen, Nature **442**(7101), 403 (2006)

T. Ezashi, P. Das, R.M. Roberts, PNAS; **102**(13), 4783–4788 (2005)

M. Gassmann, J. Fandrey, S. Bichet, M. Wartenberg, H.H. Marti, C. Bauer et al., PNAS **93**(7), 2867–72 (1996)

A.S. Gleiberman, J.M. Encinas, J.L. Mignone, T. Michurina, M.G. Rosenfeld, G. Enikolopov, Dev. Dyn. **234**(2), 413–21 (2005)

Y.S. Hwang, B.G. Chung, D. Ortmann, N. Hattori, H.C. Moeller, A. Khademhosseini, PNAS **106**(40), 16978–83 (2009)

E.J. Itskovitz, M. Schuldiner, D. Karsenti, A. Eden, O. Yanuka, M. Amit et al., Mol. Med. **6**(2), 88–95 (2000)

M.H. Johnson, Annu Rev Cell Dev Biol (2009)

J.M. Karp, J. Yeh, G. Eng, J. Fukuda, J. Blumling, K.Y. Suh et al., Lab Chip **7**(6), 786–794 (2007)

G.M. Keller, Curr. Opin. Cell Biol. **7**(6), 862 (1995)

N. Korin, A. Bransky, U. Dinnar, S. Levenberg, Lab Chip **7**(5), 611–617 (2007)

N. Korin, A. Bransky, M. Khoury, U. Dinnar, S. Levenberg, Biotechnol. Bioeng. **102**(4), 1222–30 (2009)

H.C. Moeller, M.K. Mian, S. Shrivastava, B.G. Chung, A. Khademhosseini, Biomaterials **29**(6), 752–763 (2008)

J.C. Mohr, J.J. de Pablo, S.P. Palecek, Biomaterials **27**(36), 6032 (2006)

S.J. Morrison, M. Csete, A.K. Groves, W. Melega, B. Wold, D.J. Anderson, J. Neurosci. **20**(19), 7370–76 (2000)

E.S. Ng, R.P. Davis, L. Azzola, E.G. Stanley, A.G. Elefanty, Blood **106**(5), 1601–1603 (2005)

J.S. Odorico, D.S. Kaufman, J.A. Thomson, Stem Cells **19**(3), 193–204 (2001)

J. Park, C.H. Cho, N. Parashurama, Y. Li, F. Berthiaume, M. Toner et al., Lab Chip **7**(8), 1018–28 (2007)

M.J. Powers, K. Domansky, M.R. Kaazempur, A. Kalezi, A. Capitano, A. Upadhyaya et al., Biotechnol. Bioeng. **78**(3), 257–269 (2002)

S. Provot, D. Zinyk, Y. Gunes, R. Kathri, Q. Le, H.M. Kronenberg, et al. J. Cell. Biol. **7**;**177**(3), 451–64 (2007)

R. Rajpurohit, C.J. Koch, Z. Tao, C.M. Teixeira, I.M. Shapiro, J. Cell. Physiol. **168**(2), 424–432 (1996)

P. Roy, H. Baskaran, A.W. Tilles, M.L. Yarmush, M. Toner, Ann. Biomed. Eng. **29**(11), 947–55 (2001)

D. Shweiki, A. Itin, D. Soffer, E. Keshet, Nature **359**(6398), 845 (1992)

M.C. Simon, B. Keith, Nat. Rev. Mol. Cell Biol. **9**(4), 285 (2008)

A.M. Skelley, O. Kirak, R. Jaenisch, J. Voldman, uTAS 581–583 (2007)

D. Solter, J. Gearhart, Science **283**(5407), 1468–70 (1999)

A. Spradling, B.D. Drummond, T. Kai, Nature **414**(6859), 98 (2001)

J.A. Thomson, E.J. Itskovitz, S.S. Shapiro, M.A. Waknitz, J.J. Swiergiel, V.S. Marshall et al., Science **282**(5391), 1145–47 (1998)

A. Tourovskaia, X. Figueroa-Masot, A. Folch, Lab Chip **5**(1), 14–19 (2005)

M.D. Ungrin, C. Joshi, A. Nica, C. Bauwens, P.W. Zandstra, PLoS ONE **3**(2), e1565 (2008)

L.G. Villa-Diaz, Y.S. Torisawa, T. Uchida, J. Ding, N.C. Nogueira-de-Souza, K.S. O'Shea, S. Takayama, G.D. Smith, Lab Chip **9**(12), 1749–55 (2009)

F.M. Watt, B.L. Hogan, Science **287**(5457), 1427–30 (2000)

L. Wu, D. Di Carlo, L. Lee, Biomed. Microdevices **10**(2), 197 (2008)